I R A M P
6(2), Dec. 2015, pp. 101-115

ISSN: 2229-3159

Self-Absorption Corrections to Hydrogen and Aluminum Line Profiles in Laser-Induced Plasma

DAVID M. SURMICK AND CHRISTIAN G. PARIGGER*

The University of Tennessee / University of Tennessee Space Institute, Center for Laser Applications,411 B.H. Goethert Parkway, Tullahoma, TN 37388-9700, USA
**Corresponding author E-mail: cparigge@tennessee.edu (C.G. Parigger)*

ABSTRACT: Laser-induced plasma is generated to study the Stark-broadened Balmer series hydrogen alpha line and the $3s^23p \leftrightarrow 3s^24s$ aluminum 394.4 and 396.15 nm ground state transitions. Self-absorption effects are addressed by retro-reflecting plasma emissions through the plasma prior to spectroscopic imaging in order to determine wavelength dependent correction factors. The corrected line profiles are fit using Voigt profiles to de-convolve the instrument width from the Stark-broadened line component. At a time delay of 70 ns following plasma initiation, H_α spectra show self-absorption corrections; however, the electron density, N_e, that is determined from the H_α line width remains the same. An electron number density of $2.4 \pm 0.3 \times 10^{18}$ cm^{-3} is found from the H_α line width while the line shift shows a value of $2.2 \pm 0.4 \times 10^{18}$ cm^{-3}. At similar time delays, the Al line at 394.4 nm shows a significant change under the influence of self-absorption as the spectral width reduces from 1.3 ± 0.2 to 0.9 ± 0.2 nm with a corrected N_e of $3.0 \pm 1.0 \times 10^{18}$ cm^{-3}. The Al 396.15 nm line is further distorted by the neighboring Al^+ and N^+ lines near 399.5 nm, making the self-absorption tests inconclusive for this line.

PACS Codes: 32.70.Jz, 33.70.Jg, 52.38.Mf, 52.50 Jm

Key words: Aluminum, Hydrogen, Balmer Series, Stark Broadening, Line Shapes, Voigt Profile, Laser-Induced Plasma, Laser Ablation, Laser-Induced Breakdown Spectroscopy

1. INTRODUCTION

Laser-induced plasma phenomena are of interest for studies of Stark-broadened line profiles of atomic emissions across a wide range of plasma densities and temperatures. Two of the most fundamental and important quantities in determining the state of the plasma are the electron density, N_e, and the plasma temperature, T_e, both of which may be determined using spectroscopic methods. The line width of the characteristic line profile of atomic emissions under Stark broadening shows a power law dependence on the electron density [1-3]. The temperature distribution of a local thermodynamic equilibrium plasma emission obeys a Boltzmann distribution (or Saha-Boltzmann distribution when including ions) and thus several emissions can be used with the so-called Boltzmann plot method to infer the temperature. Both of these fundamental quantities, electron density and temperature, may show spatial distributions that are helpful in shockwave diagnostics of laser-induced plasma and laser-induced breakdown events. This work focuses on a detailed analysis of line-of-sight plasma emission measurements of hydrogen Balmer series and selected aluminum lines.

Analysis of the spectroscopic line profiles for the determination of N_e is widely used for diagnostics of temporally and spatially resolved records of laser-induced plasma. In this vain, spectroscopic studies of aluminum laser ablation and aluminum plasma emission have long been of interest due to the abundance of aluminum in industrial applications [4]. Equally, accurate hydrogen line profiles continue to be of importance in the investigations of astrophysical objects [5, 6] utilizing various theory implementations and developments with parameterized Stark broadening functions dating to 1959 [7, 8]. The shock phenomena and, in general, the plasma dynamics are of interest for

studies of hypersonic expansions, including the application of advanced optical and spectroscopic diagnostics for characterization of rapidly moving shock fronts, for example, in the comparisons and scaling of large and small shockwave phenomena. Associations of the spatial variations with the temperature and N_e are of interest for the physical insight these parameters may provide into these phenomena.

Line shape diagnostics are valuable tools for analysis of spectral emissions from laser-induced plasma. This is particularly so for Stark-broadened emissions where experimental benchmarks and numerical simulations are available. The first of such studies began in the 1960's with the development of the semi-classical theory of Griem for hydrogen Stark-broadened emissions [1]. Since that time, many experiments and simulations of Stark-broadened emissions have been performed covering the 10^{14} to 10^{19} cm^{-3} range of electron densities [9-12, 31]. At larger electron densities, ion dynamics and accelerations of electrons play an important role [11] while at lower electron densities Van der Waals broadening show more prominent effects [12].

Due to the long history and numerous studies performed involving hydrogen, Stark-broadened hydrogen emissions are often used to benchmark non-hydrogenic emissions. Non-hydrogenic emissions typically show Lorentzian profiles though exact Stark broadening models are cumbersome and difficult in nature for comprehensive profile simulations. The results of computational studies are so-called Stark tables in which the Stark width of a line of interest is given at a particular density and temperature which have been rigorously experimentally validated [14, 15]. In the case of aluminum, such line shape studies began in the 1970's when stabilized arc discharge plasmas were used to benchmark Stark widths of the Al ground state transitions [16]. Subsequent simulations and experiments have been performed in which Stark broadening mechanisms at electron densities in the 10^{17} to 10^{19} cm^{-3} range were considered [17, 18-20]. We seek to work in this region while considering the entire line profile.

In this work, we investigate one aspect in the necessary steps to be able to perform the bench mark studies needed to achieve the advanced diagnostics goals; namely, how self-absorption affects the total line profile. Self-absorption occurs as the spectral emissions radiate through cooler regions of the plasma. In the cooler region, atoms are more likely to populate less excited states (ground states) and thus may absorb energy from the spectral emissions emanating from a hotter and more dense region of the plasma. During the formation of the laser-induced plasma, a hot and dense plasma kernel is formed. Shortly after the interaction of the laser pulse with the sample, the plasma begins to expand causing exterior regions of the plasma to become cooler and less dense. This creates a natural situation for self-absorption to occur, particularly at the earliest time delays from plasma formation, when the central region of the plasma is at its most dense state for standard ambient temperature and pressure (SATP), or $N_e \geq 10^{19}$ cm^{-3}.

Self-absorption manifests as a distortion of the measured line profile. As such, for diagnostics based on accurate considerations of the line profile, these distortions must be taken into account. This may be accomplished through the tabulation of a wavelength dependent experimental correction factors. A reliable, physically sound, and rather direct experimental method is to make use of a mirror to accomplish duplication the plasma, with the subsequent comparison of the plasma measured with its duplicated image to the emission of the plasma [21-24]. This is achieved through the use of a retro-reflecting mirror that directs plasma emissions back through the plasma prior to spectroscopic imaging. The experimental correction factor to be determined is given by

$$K_{corr}(\lambda) = \frac{\ln(y(\lambda))}{y(\lambda)-1} \tag{1}$$

with

$$y(\lambda) = \frac{R(\lambda)-1}{R_C(\lambda)-1} \tag{2}$$

where $R_C(\lambda)$ is the wavelength dependent ratio of the continuum for cases with and without the mirror and $R(\lambda)$ is the ratio of the line profiles. Equations 1 and 2 are a directly derived result from the equation of radiation transport for optically thin sources when evaluating the cases without and with duplication including losses from the retro-reflection [23, 24].

The plasma duplication method is only applicable when moderate self-absorption ($\tau \leq 1$) is present and is also limited for non-isolated spectral lines with interfering neighboring emissions. This mostly applies to optically thin or nearly optically thin plasma emissions. For strong self-absorption, the ratio modeling becomes complicated and is no longer straight forward in its application [26]. A non-quantitative observation that is often associated with strong self-absorption is line self-reversal, which most commonly occurs for ground state transitions in laser-induced plasma. Here, we present experimentally determined corrections to atomic emission line profiles from laser-induced plasma following ablation of an aluminum alloy target in a controlled hydrogen/nitrogen gas mixture at atmospheric pressure. This mixture is selected to establish potential correlations between the hydrogen and aluminum emissions. A plane mirror coupled with a lens is used to duplicate the signal and re-direct through the plasma prior to spectroscopic imaging. Subsequently, the corrected emission profiles are analyzed in an effort to evaluate how self-absorption affects the N_e diagnostics. This is done in an effort to investigate self-absorption of the isolated hydrogen Balmer series alpha line and also investigate the validity of applying the experimental duplication method to ground state Al transitions in a situation that approaches the strong self-absorption limit.

2. EXPERIMENTAL METHODOLOGY

Laser-induced plasma was studied spectroscopically following plasma initiation from focused 1064 nm, Nd:YAG laser radiation. Self-absorption effects are studied by re-imaging the plasma onto itself prior to spectroscopic imaging through use of a plane, reflecting mirror. The plasma was initiated by focusing 120 mJ, 14 ns pulsed laser radiation through the window of a gas cell chamber onto the target surface. A 125 mm focal length UV-fused silica plano-convex lens was used. The target surface was an aluminum 6061 alloy sample approximately 2×2 cm square that was cleaned in an acetone/methanol bath prior to laser ablation to remove surface contaminants. The breakdown event was imaged onto the slit of a 0.64 meter Jobin-Yvon, HR640 Czerny Turner style spectrometer installed with a 1200 grooves/mm grating. The gas cell was filled with 90% ultra-high purity (UHP, 99.999% pure) hydrogen gas and 10% UHP nitrogen gas and was evacuated with a mechanical/diffusion pump system to a pressure of 10^{-3} Pa (1×10^{-5} Torr) prior to filling the chamber volume with the desired gas atmospheres.

The plasma emissions were recorded with an Andor iStar intensified charge couple device (ICCD). The detector was a rectangular array of pixels. When coupled with the spectrometer, the horizontal arrays of pixels are used to record spectrally resolved data. In our experimental arrangement, with a vertically incident laser beam that is perpendicular to the direction in which the slit is opened, the vertical pixels on the detector recorded spatially resolved data along the height of the spectrometer slit. The extent of the pixels on the ICCD is 13.6 × 13.6 μm. This resulted in a spectral instrument resolution of approximately 0.15 nm for the selected slit width of 50 ìm. Groups of 8 vertical rows were data-binned to achieve a spatial instrument resolution of 0.108 mm along the slit height. The imaging characteristics of the system were such that the plasma imaged onto the ICCD at 1.05:1. The spectral and spatial resolutions (or spectral and spatial instrument resolutions) are the important figures of merit, and for completeness we included the actual slit width that was used. It is the spectral and spatial resolutions that are of physical significance. Our instrument is capable of resolving digital data at a resolution much better (typically a factor of 3 to 5 better) due to the ICCD dimensions and the chosen spectrometer. However, the spectral resolution is determined by the slit width, the spatial resolution by the binning. Both of which are affected by the modulation transfer function, especially of the intensifier.

The self-absorption effects were studied using a plane, reflecting mirror and a lens to reflect the plasma onto itself prior to spectroscopic imaging. The plasma was first imaged onto the plane reflecting mirror. This image was then passed back through the lens and onto the plasma. The plasma and its duplicate were then imaged onto the spectrometer slit as is usually done in a typical laser-induced breakdown spectroscopy experiment [25]. A block diagram of this section of the apparatus is shown in Figure 1. The lenses used to image the plasma onto the mirror and the plasma and its duplicate image onto the spectrometer slit were identical and consisted of uncoated, UV-fused silica singlets 5 cm in diameter with a focal length of 100 mm. To aid in the alignment of the apparatus, the mirror and the lens used to image the plasma onto the mirror were positioned with 5-axis Gimbel mounts for fine adjustments.

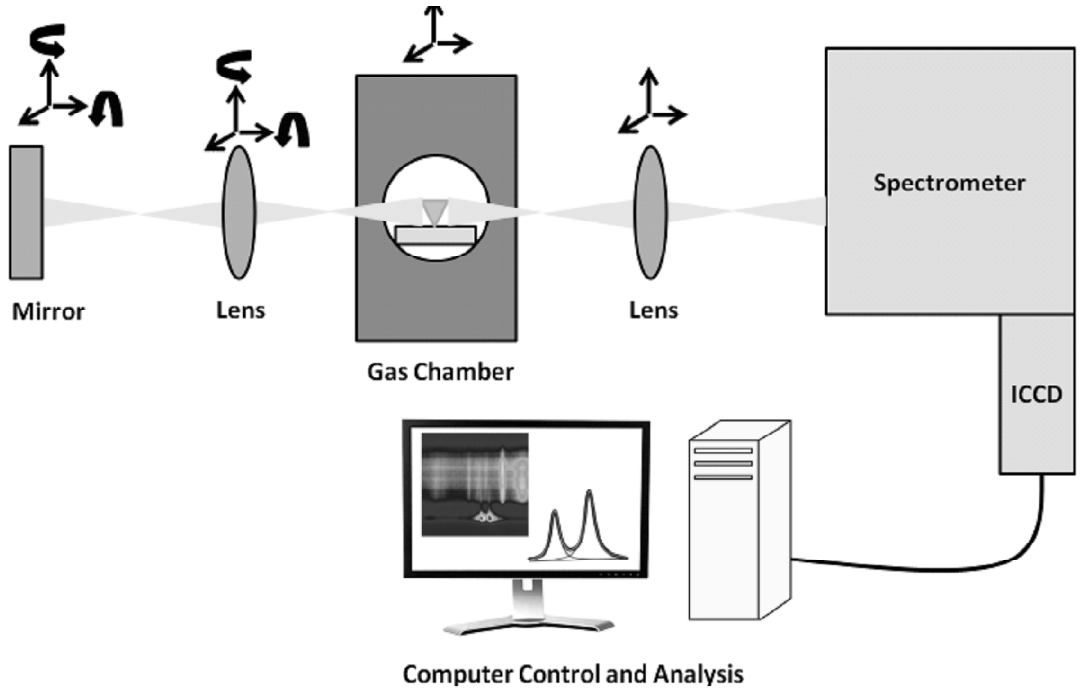

Figure 1: Block diagram of the self-absorption section of the experimental apparatus

The alignment of the self-absorption apparatus is a delicate and vital component of this work given the spatial resolution of the ICCD. To aid in this procedure, the lens used to image the plasma and its duplicate was fixed at its position such that it properly produced a focused image on the spectrometer slit and the ICCD. This position corresponded to the location equivalent to the distance of $2\times$ the focal length of the lens in relation to the spectrometer slit and $2\times$ the back focal length (93.7 mm) of the lens in relation to the breakdown plasma, taking into account the thick lens approximation. Likewise, the lens used to image the plasma onto the plane mirror was initially placed at a distance of $2\times$ the focal length of the lens in relation to the mirror and $2\times$ the back focal length of the lens in relation to the breakdown plasma, with the curved surface of the lens facing the plane mirror.

The best possible alignment was achieved by fine adjustments of both lenses and the mirror. The sample surface was taken to be fixed and was aligned such that it was as close as possible to the center of the optical axis connecting the lenses, mirror, and spectrometer slit. The alignment was checked using zero order imaging with the spectrometer. A sufficient alignment was considered to be one in which ICCD images collected with and without the duplicating mirror were nearly identical. Further fine adjustments were made by comparing collected ICCD spectra with and without the duplicating mirror such that the ratio was as large as possible, with an ideal ratio limit of 2. These adjustments were made by viewing the Balmer series hydrogen beta line, H_α, at a time delay of 10 μs in SATP laboratory air breakdown. For this time delay, self-absorption for this spectral line is likely to be insignificant [27, 28].

In practice, the mirror and lens used to image the plasma onto the mirror were adjusted the most and the lens used to image the plasma onto the spectrometer was only adjusted when absolutely necessary. This procedure was used since the goal was to duplicate the plasma imaging process that would normally occur in a LIBS experiment. The initial alignment procedure was performed without the gas chamber in place. The best practical ratio of cases of measured spectra with and without the duplicating mirror in this arrangement was 1.67:1 because of losses at the mirror and the lens used to image the plasma onto the mirror. Due to the presence of the windows at the gas chamber, this ratio is further reduced when performing the ablation experiments in the controlled gas atmosphere. As such, a measured ratio between 1.25 and 1.4 was considered acceptable given the optical losses of the emission signal.

Spectra of interest were recorded at systematically varied time delays, τ_{delay}, starting from 10 ns following plasma initiation up to a delay of 100 ns. The selected gate width for each measurement was 5 ns. The aluminum

lines that were studied in the current effort are the ground state $3s^23p \leftrightarrow 3s^24s$ transitions, which are split due to spin-orbit coupling of the ground state with j=1/2 for the 394.4 nm emission and j=3/2 for the 396.15 nm emission. Figures 2 and 3 show examples of measured ICCD spectra for the Balmer series hydrogen alpha line, H_α, and the aluminum line spectra of interest, respectively, at a delay of 70 ns. The slight variation of recorded signals near the slit height of 8.5 mm in Fig. 2, and the apparent slight signal modulations are not further investigated because these details do not affect the self-absorption corrections and conclusions. Fig. 3 also shows significant contributions from a nitrogen ion line, N^+, at 399.5 nm and near the slit height range of 6 to 8 mm. These two images, recorded for different spectrometer settings, show the spatial localization with respect to the slit height and wavelength range of the emitted spectra.

The source of the hydrogen and nitrogen ion (particularly N^+ at 399.5 nm) emissions are from the gas atmosphere. The source of the aluminum is from the surface of the sample target. As such, the hydrogen and ionic nitrogen emissions encompass a greater spatial distribution while the aluminum emissions are confined to a small region close to the sample surface. This is due primarily to the choice of focal position for the Nd:YAG laser radiation. The sample and laser focus were purposefully positioned such that the laser focus was outside of the sample surface. Separate breakdowns were initiated in the gas atmosphere from the surface breakdown so that both surface breakdown and gas breakdown could be studied independently as well as simultaneously to elucidate cross over effects.

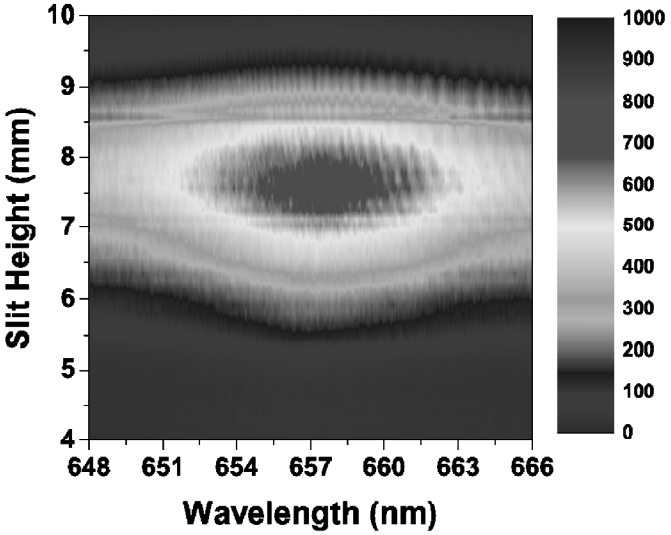

Figure 2: Recorded ICCD image of H_α spectra along the spectrometer slit height at τ_{delay} = 70 ns

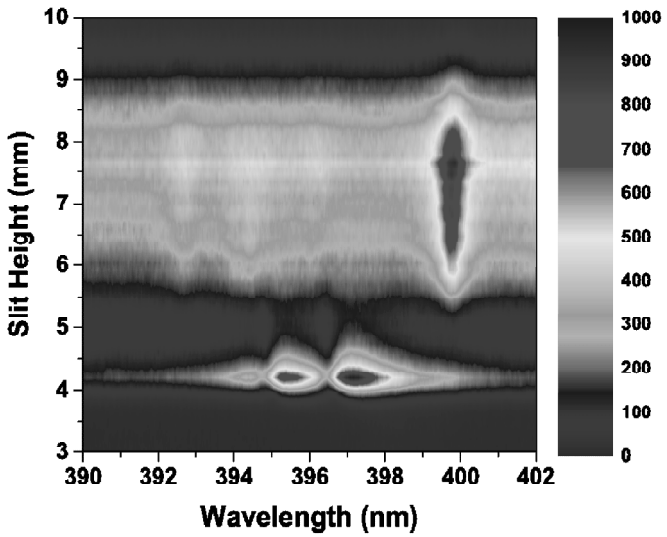

Figure3: Recorded ICCD image of Al 394.4 and 396.15 nm and N^+ 399.5 nm spectra along the spectrometer slit height at τ_{delay} = 70 ns

The collected spectra are analyzed to determine the experimental correction factor given in Equation 1 and, subsequently, the self-absorption profiles are considered for determination of N_e. Prior to the line profile analysis, the measured spectra are calibrated for the spectrometer detector arrangement wavelength and intensity responses.

3. RESULTS AND DISCUSSION

For the determination of the electron density in the presence of self-absorption, one must first correct the spectroscopic line profiles using the experimental correction factors. This requires a fitting process to the collected data. In our analysis procedure, first, measured line profiles with and without the doubling mirror are fit with Voigt profiles, then the experimental correction factors are tabulated, followed by Voigt fitting to the corrected profile a second time, the correction factors are applied by $K_{corr}(\lambda) \times S(\lambda)$, and comparisons with theory are made to determine the electron density, N_e.

By definition, the Voigt profile is a convolution of Gaussian and Lorentzian line profiles and, as such, fitting to a Voigt profile allows one to simultaneously consider Gaussian and Lorentzian aspects of a spectroscopic profile.

The Gaussian components of the line profile are taken to be the instrument width of the spectrometer-detector arrangement. The residual Doppler width due to the thermal motion of the plasma particles can also be combined in a single Gaussian line profile. If one takes the Lorentzian component of the Voigt profile to represent an approximation to the Stark-broadened profile of the line, the electron density can be determined from the line width that was de-convolved from the Gaussian contributions. In the analysis of hydrogen alpha emission lines, tabulated profiles have been used previously [29] but for practical purposes Lorentzian fitting is applied for this Stark-broadened line. Of course, there are slight differences in the wings over and above the distortions due to self-absorption. Modeling of self-absorbed lines can be accomplished as recently outlined [30, 31] using the Lorentzian profiles convolved with the instrumental Gaussian profile. This methodology of fitting Lorentzians and Gaussians to obtain the Voigt profiles is utilized in the analysis of the hydrogen and aluminum lines discussed in detail below.

3.1. Voigt profile fitting

Numerical simulations of Voigt profiles is an extensive sub-field of study in itself [32-35]. We do not claim or seek to employ a novel method for simulating the Voigt profiles, rather we utilize a method that has sufficient accuracy and computational speed that best matches the spectral resolution, $\delta\lambda$ = 0.15 nm, of our experimental apparatus. Most numerical simulations of Voigt profiles center around the Fadeeva function, $W(z)$, also called the the plasma dispersion function or complex complimentary error function [36, 37],

$$W(z) = e^{-z^2} erfc\{-iz\}, \tag{3}$$

for complex arguments, $z = x + iy$ with $x, y \in R$. The real part of this function reduces to the well known integral form of the Voigt profile,

$$V(x,y) = \int_{-\infty}^{\infty} \frac{e^{-t^2} dt}{y^2 + (x-t)^2}. \tag{4}$$

For appropriate choice of x,

$$x = \frac{\lambda - \lambda_0}{w_g} 2\sqrt{\ln 2}, \tag{5}$$

and y,

$$y = \frac{w_l}{w_g} \sqrt{\ln 2}, \tag{6}$$

the correct weighting of the Lorentzian and Gaussian components are obtained, and the line profiles are constructed from the line width components w_l and w_g, respectively.

Calculation of the Voigt profile is implemented using the methods of Zahgloul *et al.*, termed Algorithm 916 [34]. In this method the Voigt integral is solved by splitting it into line segments. This affords for rapid series convergence for the spectral resolutions encountered in this work, particularly in the upper-half complex plane that is of interest for spectroscopy applications.

Fitting to the measured spectra is performed using the non-linear least squares Trust-Region algorithm [38, 39]. The fit parameters were the amplitude, Lorentzian width, and peak shift, as well as a linear baseline offset. The Gaussian width is held constant at the value of the spectral resolution, $\delta\lambda$, of the apparatus. This value was determined during spectral calibrations. The linear baseline offset is used to approximate the spectral continuum that is measured. A linear offset is assumed to be adequate for the considered spectral ranges of the order of 20 nm.

In the case of fitting to aluminum spectral emissions, multiple lines were observed simultaneously. This is due to the spectral separation of the spin-orbit splitting of the $3s^23p \leftrightarrow 3s^24s$ Al ground state transition and also due to

the presence of nitrogen lines originating from the 10% nitrogen gas atmosphere component. In these cases, the multiple lines needed to be fit simultaneously. This was accomplished by fitting a sum of Voigt profiles equal to the number of resolved peaks, *i.e.*, if there were two resolved peaks the fitting function would be a sum of two Voigt profiles in addition to the linear baseline offset. Figure 4 shows a sample fit to the two Al lines of interest, with unperturbed line positions at 394.4 and 396.15 nm.

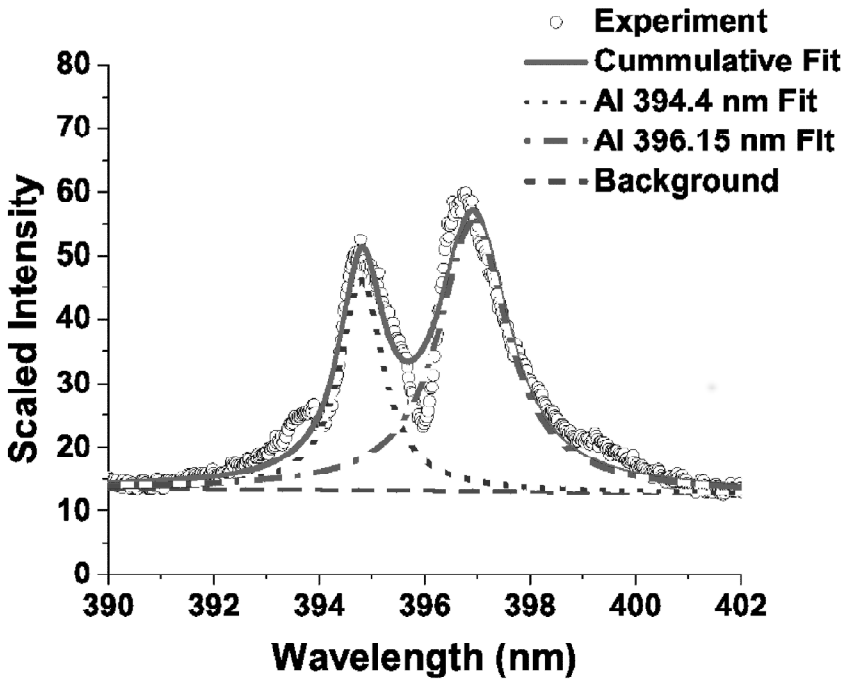

Figure 4: Voigt fit to Al 394.4 and 396.15 nm lines at a 70 ns delay and 4.35 mm slit height

The widths of the two lines shown in Figure 4 are 1.3 ± 0.2 and 1.45 ± 0.2 nm for the Al 394.4 and 396.15 nm lines, respectively. The corresponding electron densities N_e for these lines are of the order of $10^{18}cm^{-3}$, with the exact values to be determined following the hydrogen alpha line profile analysis and self-absorption corrections. The corrected aluminum profiles are communicated and further discussed in Section 3.3, see Figure 9. The deviation from the expected factor of 2 intensity ratio and the agreement of Stark widths within multiplets of optically thin lines [40] can be due to both self-absorption and spatially inhomogeneous distributions along the line-of-sight measurements in the expanding laser-induced plasma. The spatially inhomogeneous distribution can be addressed as communicated in very recent work using Abel and/or Radon inversion techniques [41, 42]. In a recent review, the recorded aluminum ratio in laser-induced plasma was reported to deviate from the exact factor of 2 [43].

3.2. H_α self-absorption correction factors and N_e determination

The self-absorption experimental correction factors are determined as a direct result of the fitting process employed. For completeness, the same fitting procedures used for fitting the aluminum lines were applied for the H-alpha analysis although minimal instrumental width effects are expected for Stark widths of the order of 10 nm. The fits were performed using a linear, wavelength dependent baseline offset in addition to the Voigt profiles used to simulate the emission lines. In this way $R_c(\lambda)$, taken to be the fitted offset, and $R(\lambda)$, taken to be the fitted Voigt profile without the offset, are readily determined for use in Equations 1 and 2. Figure 5 shows a fitted H_α spectrum at a slit height of 5.98 mm and for τ_{delay} = 70 ns to be used for self-absorption corrections. The corresponding calculated correction is shown in Fig. 6. One should note, the self-absorption approach presented in the introduction implies that the correction factor must always be greater than one.

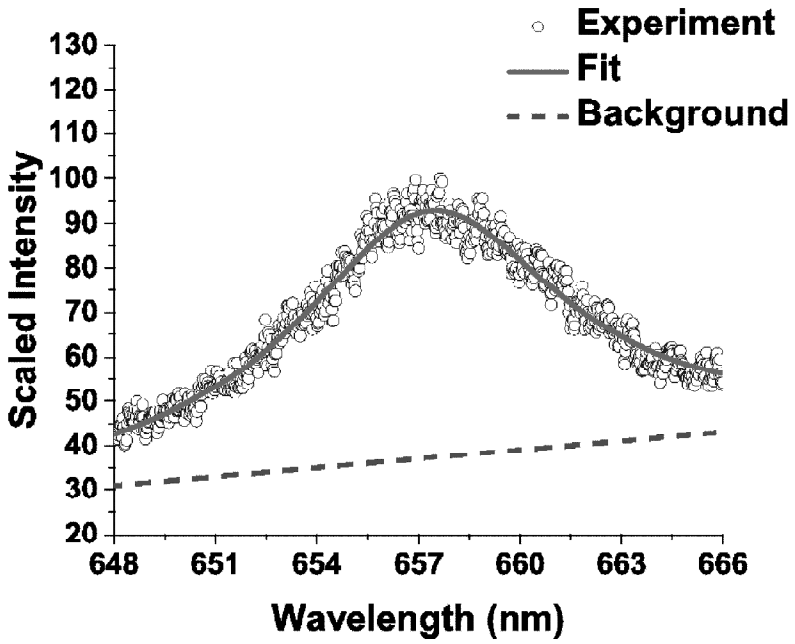

Figure 5: Measured H_α spectrum; τ_{delay} = 70 ns and a slit height of 5.98 mm. The width is 9.7 nm

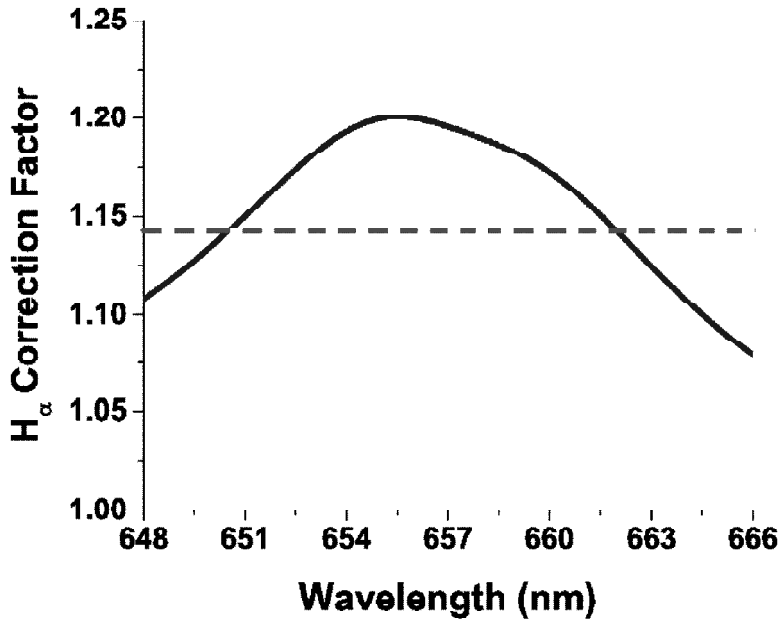

Figure 6: Experimental correction factor for H_α spectrum collected at τ_{delay} = 70 ns and a slit height of 5.98 mm. The average 1.14, indicated by the dashed line

Also indicated in the figure, via the red line, is the average of the self-absorption correction factor, which in this case shows a value of 1.14. Though the average is not used when correcting for self-absorption. It aids in providing a metric showing the general level of self-absorption that may or may not be present.

The resulting corrected H_α profile is shown in Figure 7. From the similar scale used to represent the measured *vs.* self-absorption corrected profiles, irrespective of any change in the width of the profile, on can confirm that the entire profile has indeed changed under the influence of self-absorption. Comparison of Figures 5 and 7 reveals that the widths change from 9.9 ± 0.2 nm to 10.0 ± 0.2 nm.

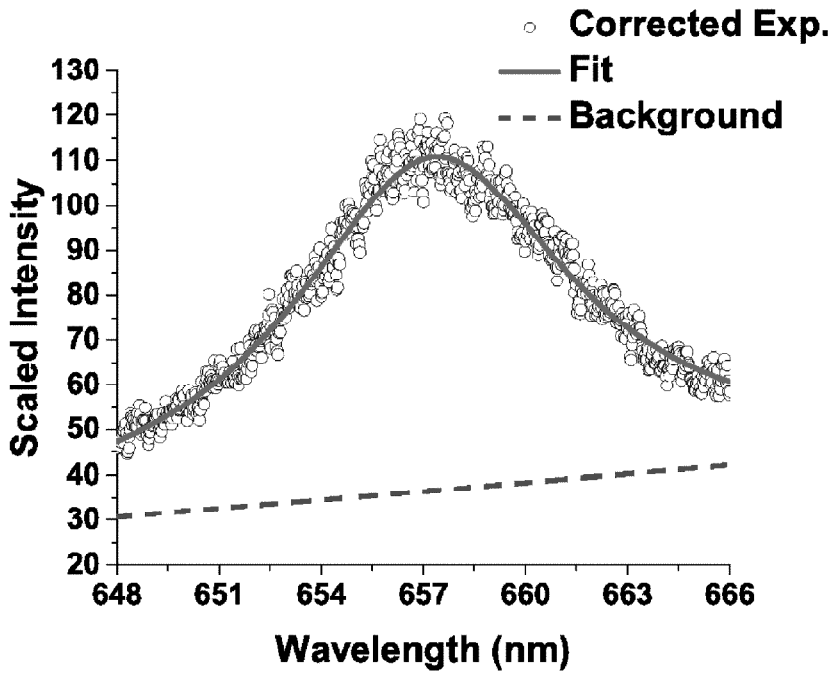

Figure 7: Self-absorption corrected H_α spectrum at τ_{delay} = 70 ns and a slit height of 5.98 mm. The width is 10.0 nm

The correction factors displayed in Figure 6 indicate that the greatest correction occurs near the line center and falls off in the line wings. One can also clearly see that the correction factor does not inherently show a symmetric profile. This is not unexpected due to the nature of Stark broadening. The H_α causing the absorption to take place is likely to be at a lower temperature and N_e, therefore, it will exhibit a smaller Stark width and shift resulting in an asymmetric absorption of the measured profile, leading to an asymmetric self-absorption correction factor.

Once the profiles are corrected for self-absorption, the electron density can be determined. We chose to use a method that includes necessary alterations to the semi-classical theory for Stark broadening of hydrogen Balmer series spectra. Specifically, we employ empirically developed formulas [44] for the width the H_α line, which was developed from accurately collected Balmer series spectra from a laser-induced plasma and subsequently analyzed using the convergent theory of Oks [9]. The empirical formulas from Ref. [44] for the H_α Stark width and shift are given in Equations 7 and 8, respectively. In the current effort, we only consider the self-absorption effects on N_e found from the width of the H_α line since the shift is expected to be unaffected by moderate self-absorption, *i.e.*, no line reversal. Rather, N_e found from the shift may serve as an additional indicator as to whether the self-absorption affects have been accurately corrected. The corrected N_e corresponding to the width of the line in Fig. 6 amounts to $2.4 \pm 0.3 \times 10^{18}$ cm^{-3}. The value of the line shift is 1.1 ± 0.2 nm in the uncorrected fit and is 1.0 ± 0.2 nm in the corrected fit. Though a small change in the shift does occur, this is well within the experimental error margin of 0.2 nm and thus the shift of the H_α line indicates practically the same electron density N_e of $2.2 \pm 0.4 \times 10^{18}$ cm^{-3}. When considered with the error margin, which includes contributions from the fitting process as well as the accuracy of the experiment, the H_α line shift and line width indicate the same electron density

$$\Delta w[\text{nm}] = 1.31 \times \left(\frac{N_e[\text{cm}^{-3}]}{10^{17}} \right)^{0.64 \pm 0.03} \tag{7}$$

$$\Delta \delta[\text{nm}] = 0.055 \times \left(\frac{N_e[\text{cm}^{-3}]}{10^{17}} \right)^{0.97 \pm 0.03} \tag{8}$$

The average correction factor of 1.14 would seem to indicate that a distortion to the profile has occurred. The width of the profile and the inferred N_e are unchanged due to considerations of the self-absorption profile of the H_α line at τ_{delay} = 70 ns. In fact, the line width is shown to increase very slightly when the $H_á$ line profile was corrected for self-absorption; however, with the mentioned error margins, this increase has a minimal impact on the determined N_e.

The spatial variation of the experimental self-absorption correction is displayed in Table 1. The average of the experimental self-absorption correction factor is indicated as the metric of the extent of self-absorption, yet again, the theoretical correction factor for the introduced self-absorption approach must be greater than one. Values of the average that are significantly less than one are not physically meaningful. As such, we only indicate values that are close to one. The limited spatial scope of Table 1 in view of the rest of the figures presented (≈ 1.5 *vs.* ≈ 6 mm) is due to the difficulty in aligning the self-absorption apparatus. The methods used to align the self-absorption optics allows one to align the optics within 0.2 mm. This is due to the scale of the fine adjustment options on the physical optical comments used. Consequently, the error for both the uncorrected and self-absorption corrected line widths in Tab. 1 is 0.2 nm. The error margin for N_e is indicated along with the determined, self-absorption corrected value in the final column of the table.

Table 1
Spatial variation of the average experimental correction factor. The middle two columns show the original and corrected widths of the H_α profiles and the final column shows the inferred electron density

Height (nm)	K_{corr} *Avg*	$H_\alpha \Delta w$ *(nm)*	$H_\alpha \Delta w$ *Corr (nm)*	$N_e \times 10^{17}$ cm^{-3}
5.44	0.94	7.4	5.3	8.8 ± 3.0
5.66	1.12	8.4	8.8	19.7 ± 3.0
5.88	1.06	9.2	8.3	17.9 ± 3.0
6.09	1.05	9.8	9.8	23.3 ± 3.0
6.31	1.01	10.5	10.4	25.5 ± 3.0
6.53	0.91	11.1	10.0	23.9 ± 3.0
6.75	0.86	11.6	9.4	21.7 ± 3.0

The values at the extreme vertical positions of the plasma given Table 1 show the largest changes due to self-absorption. Though self-absorption may indicate such an extreme distortion, with the line width reduced by 2.0 nm, it is more likely that these values are affected by misalignment of the mirror, which is indicated by the average self-absorption correction factor being less than 1, this is most significant in the final entry of the table which shows a correction factor of 0.86. The effects of self-absorption are most prominent between slit heights of 5.98 and 6.09 mm. With the exception of the first, third, and final entries in Table 1, the H_α line widths change inconsequentially within the experimental error margins under self-absorption effects.

While we report no changes in the widths and the parameter of interest, N_e, it is important to note that the entire profile has been changed due to the application of the self-absorption correction factor. Rather than categorically concluding that self-absorption is insignificant, this result shows that the H_α line-width diagnostic is weakly dependent on self-absorption affects at the given conditions. One should not take the H_α results to mean that all other measured lines will not be affected due to self-absorption. A complete self-absorption analysis should be performed for each line of interest. One must remember that ground state transitions are more likely to experience distortions due to self-absorption. We note here that the hydrogen Balmer series ($n_{upper} \geq 3$ to n = 2 transitions) have a lower energy level of -3.4 eV which is relatively far from the ground state of -13.6 eV for hydrogen.

Previous studies have shown that the self-absorption is important for H_α emissions in laser induced plasma by comparing H_α emissions to the continuum following laser ablation of an ice surface [31] and also through comparisons to N^+ emissions in nominal air breakdown plasma [45]. The former study indicated strong self-absorption, *i.e.*, line

reversal, for densities in excess of 6×10^{18} cm^{-3}. The latter study showed that marginal self-absorption may be possible due to differences between N_e found from N^+ spectra at 648.2 and 661.1 nm *vs.* H_α emissions. The results of that worked showed electron densities inferred from N^+ and H_α to amount to 1.4 and 2×10^{18} cm^{-3}, respectively. While the mentioned difference should not be ignored, the comparison of ions and neutral emissions of two different species in a laser-induced plasma as a test for self-absorption also must consider local thermodynamic equilibrium. When possible, a preferred method of testing the self-absorption is through comparisons of different N_e diagnostics from the same line, such as the shift *vs.* the width of the H_α line or the peak separation *vs.* the H_β line width [28]. The latter has a limited scope of applicability due to the inherent asymmetry and relatively large spectral width with respect to a 20 nm spectral window of the H_β line for N_e greater than 0.5×10^{18} cm^{-3}.

3.3. Self-absorption correction and N_e of the aluminum lines

The aluminum lines that are to be considered as part of future benchmark mark studies are ground state transitions, having line portions at 394.4 and 396.15 nm, respectively. Self-absorption effects of these lines were investigated in the same manner as with the H_α line. Figure 8 shows the resulting correction factor from performing the self-absorption analysis on the Al spectra displayed in Fig. 4 which is at a slit height of 4.35 mm. Peaks are visible near the line centers of the two lines (194.4 and 396.15 nm). The wings of each line dip well below 1 and tend toward 1 at the edge of the profile. This reflects the difficulty in determining the ratio of the continuum due to the presence of significantly overlapping line profiles, which interfere most significantly in the region between 393 and 397 nm. In general, it is difficult to accurately determine the ratios of the continuum due to the relatively narrow spectral viewing regions used in the present effort. Figure 9 displays the results of applying the correction factor shown in Fig. 8. The corrected Al lines widths are 0.9 ± 0.2 and 1.4 ± 0.2 nm for the 394.4 and 396.15 nm lines, respectively.

The Al 394.4 nm line width is significantly reduced, which is congruent with a ground state transition emitting from a plasma with an N_e greater than 2×10^{18} cm^{-3}. The Al 396.15 nm line, however, shows a very small change under self-absorption corrections. This is likely due to influences from a grouping of unresolved lines including influences from the N^+ transition at 399.5 nm as well as from Al^+ ions at 397.99 and 399.48 nm. This is noticeable as a small "lump" on the edge of the experimental trace of 396.15 nm line in Fig. 9 between 397.5 and 399.5 nm. This causes the 396.15 nm line to be additionally broadened and makes the determination of the true level of the Stark broadening for the Al 396.15 nm a relatively difficult task without a further increase in the spectral resolution.

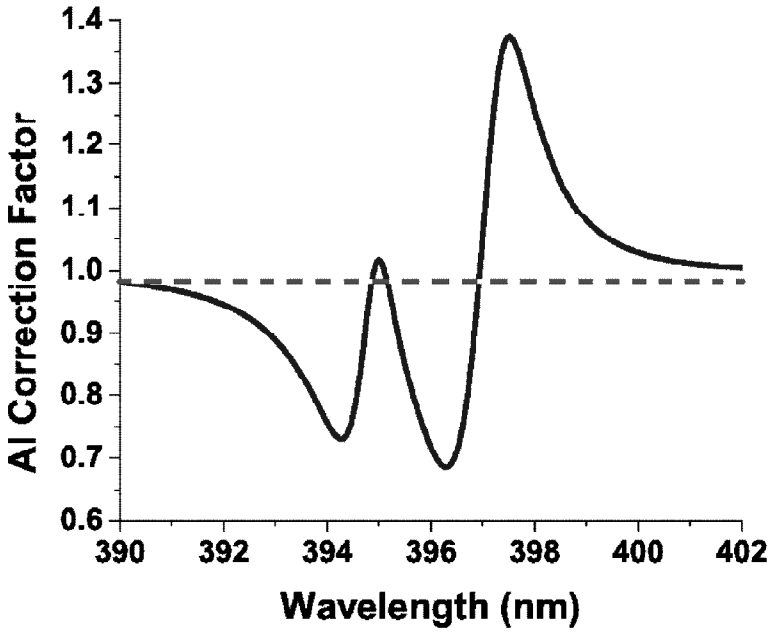

Figure 8: Experimental correction factor for Al 394.4 and 396.15 nm spectra collected at τ_{delay} = 70 ns, slit height of 4.35 mm. The average of 0.98 is indicated by the dashed line

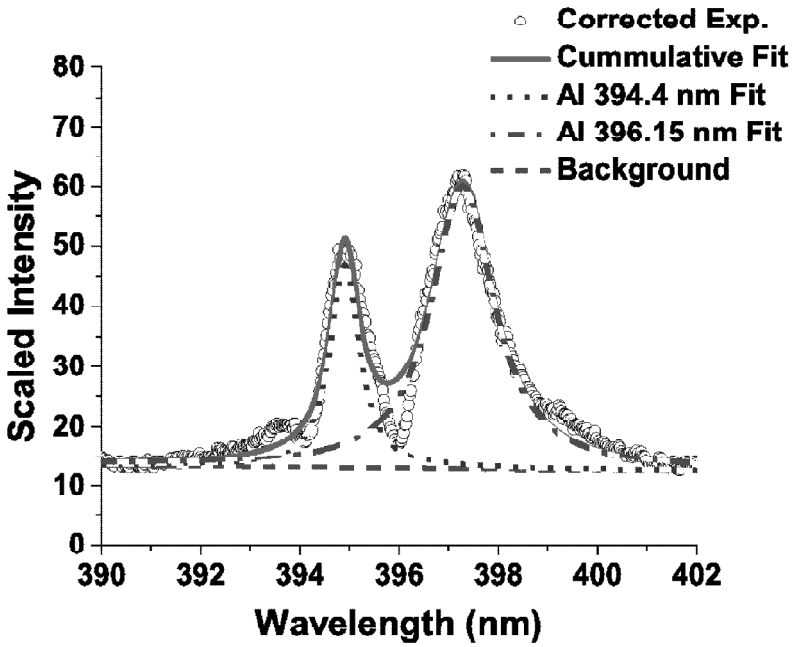

Figure 9: Self-absorption corrected Al 394.4 and 396.15 nm spectra at τ_{delay} = 70 ns; slit height: 4.35 mm

An increase in spectral resolution, in turn, would decrease the recorded spectral range when using the detector arrangement and would make determining the ratio of the continuum a more difficult task.

The electron density as inferred from the two aluminum lines may be indicated by previous experimental efforts involving Stark broadening measurements of the Al ground state transitions at N_e greater than 10^{18} cm^{-3} [46, 18]. The corrected N_e for the Al 394.4 nm shows a value of $3.0 \pm 1.0 \times 10^{18}$ cm^{-3} while the Al 396.15 nm line shows an N_e of $8.0 \pm 2.5 \times 10^{18}$ cm^{-3}. Though it is not expected nor required for the two Al transitions to have the same width, the two lines should show the same N_e after being corrected for self-absorption. The 2.5 × greater N_e indicated by the 396.15 nm line than the 394.4 nm line would imply that the 396.15 nm line experienced additional broadening due to the grouping of unresolved lines near 399.5 nm. Such a consideration makes the self-absorption tests inconclusive for the Al 396.15 nm line. This trend was also previously observed [46], and it was attributed to self-absorption effects due to the considerable difference in the computed $N_e \approx 33$ *vs.*4.0×10^{18} cm^{-3}at a 200 ns time delay in air breakdown plasma. The conclusion of that work was that the Al 396.15 nm likely experienced greater self-absorption than 394.4 nm line. While this may be possible, the current effort shows that further work would be needed to support such a statement.

In regards to the limitations of the duplication method, the investigated Al lines would appear to exceed the strong self-absorption limit due to the presence of slight line self-reversals near the two unperturbed Al lines centers as seen in Figure 4. While the strong self-absorption limit is a difficult bound to overcome experimentally, the presented results would seem to indicate that the plasma duplication method may very well be applicable to some instances of moderately strong self-absorption, although plasma emission and line shape modeling is necessary. Indeed, recent communications have shown that self-reversed H_α can be addressed with the application of Abel inversion in combination with the plasma duplication method [49, 50]. Plasma emission models in laser-induced plasma are often complicated due to the transient and inhomogeneous nature of the plasma and represents an exciting area of further fundamental research. The further need for this research does however present many challenges in study the early time evolution of laser ablation plasma emissions. One may also potentially consider self-reversed line profiles using the escape factor model which describes the emission of a particle based off of its probability to escape an opaque emission source [51]. Application of a detailed fitting procedure with this model, coupled with a detailed application of the plasma duplication method, may provide insight into the presented experimental results.

One might advance this work further by a detailed analysis of the profile of a Stark-broadened emission from a laser-induced plasma. In the present work, we have considered the use of a Voigt profile with a Lorentzian component to approximate the Stark contribution. The profile of atomic emissions under collisions of charged particles actually shows a Holtsmark distribution for each type of charged particle (protons, electrons, positrons, *et c.*) interaction [47]. The sum of these distributions gives the total line profile under Stark broadening. As such one should really consider the use of a Holtsmark profile or the convolution of a Holtsmark profile with a Lorentzian and Gaussian profile, which has recently been investigated [48] for both the hydrogen and aluminum lines to be studied. Such considerations would be necessary for future efforts in bench mark studies of the Stark-broadened Al line, especially for potential use in the early temporal evolution of laser-induced plasma when the electron density N_e is at its greatest. At these time delays, laser-induced plasma and laser ablation of metal targets are useful for studying rapidly expanding shock waves are of interest as surrogates for studies of large and meso-scale explosives events.

4. CONCLUSIONS

We have presented the results of self-absorption corrections to measured spatially and temporally resolved H_α and Al spectra. The self-absorption phenomena were studied by duplicating the plasma emission prior to spectroscopic imaging through the use of a retro-reflecting mirror and a singlet lens. A wavelength dependent correction was calculated and applied to each measured emission profile. The electron density of laser-induced plasma was determined in the first 100 ns following ablation of an aluminum target in a hydrogen gas atmosphere. Fitting of the measured spectroscopic profiles was used to aid in the determination of the wavelength dependent ratios of the measured profiles and of the continua for cases with and without the retro-reflecting mirror, which were used to tabulate the correction factors. The spectra were fit using Voigt profiles so that the instrument width, the Gaussian component, could be de-convolved from the Stark-broadened component, approximated as the Lorentzian component of the Voigt profile.

For spectra investigated at a time delay of 70 ns and a slit height in the region around 6 mm and 2 mm away from the Al target surface, the wavelength dependent corrections showed a change in the overall profile of the measured H_α line; however, the width diagnostic for the N_e causes only a minuscule change at most due to self-absorption influences for the densities encountered in this work, $N_e \approx 2\times10^{18}$ cm^{-3}. Self-absorption diagnostics with the retro-reflecting mirror apparatus were also applied to Al ground state emissions observed at 394.4 and 396.15 nm, for a time delay of 70 ns and a slit height of 4.35 mm and ≈ 0.4 mm away from the target surface. The Al 394.4 nm line showed a considerable line profile change when self-absorption distortions were taken into account. The line width of the profile decreased from 1.3 to 0.9 nm resulting in the electron density of 3×10^{18} cm^{-3}. The Al 396.15 nm line experienced little reduction from its original line width of 1.45 nm when corrected for self-absorption. This is likely a result of the additional distortions to this line from the neighboring, unresolved N^+ and Al^+ emissions. In this work, we imply in the introduction by indicating the correction factors that the study does not apply for opaque or optically thick scenarios. In an extension to the current experimental studies, one would ideally apply de-convolution algorithms for spatial and temporal mapping from the line-of-sight measurements. However, our recent work indicates that the technique for self-absorption corrections can be applied for plasma emissions that include line-reversal self-absorption effects, e.g., for the hydrogen Balmer emission lines studied with the inclusion of Abel inversion techniques [49, 50].

Acknowledgments

The authors thank the Center for Laser Applications and the University of Tennessee for support of this work.

References

[1] H.R. Griem, Plasma Spectroscopy, McGraw-Hill, New York, 1965.

[2] H.R. Griem, Spectral Line Broadening by Plasmas, Academic Press, New York, 1974.

[3] H.J. Kunze, Introduction to Plasma Spectroscopy, Spring-Verlag, Berlin, 2009.

[4] A.K. Rai, F. Yueh, J.P. Singh, Appl. Opt. 42 (2003) 2078-2084.

[5] C. Stehlé, Astron. Astrophys. Suppl. Ser. 104 (1994) 509–527.

[6] F. Clausset, C. Stehlé, M.-C. Artru, Astron. Astrophys. 287 (1994) 666-675.

[7] A.B. Underhill, J.H. Waddell, National Bureau of Standards, Circular 603 (1959).

[8] H.R. Griem, A.C. Kolb, K.Y. Shen, Phys. Rev. 116 (1959) 4–15.

[9] C.G. Parigger, D.H. Plemmons, E. Oks, Appl. Opt. 42 (2003) 5992–6000.

[10] M.A. Gigosos, M.A. Gonzaleź, V. Cardeñoso, Spectrochim. Acta Part B 58 (2003) 1489–1504.

[11] E. Oks, Stark Broadening of Hydrogen and Hydrogenlike Spectral Lines in Plasmas: The Physical Insight, Alpha Science Int., Oxford, 2006.

[12] N. Konjević, M. Ivković, N. Sakan, Spectrochim. Acta Part B 76 (2006) 16–26.

[13] C.G. Parigger, D.M. Surmick, G. Gautam, A.M. EL Sheribini, Opt. Lett. 40 (2015) 3436–3439.

[14] N. Konjević, W.L. Wiese, J. Phys. Chem. Ref. Data 19 (1990) 1307–1350.

[15] N. Konjević, A. Lesage, J. Fuhr, W.L. Wiese, J. Phys. Chem. Ref. Data 31 (2002) 819–927.

[16] C. Fleurier, S. Sahal-Brechot, J. Chapelle, J. Phys. B: Atom. Molec. Phys. 10 (1977) 3435–3441.

[17] M.S. Dimitrijević, S. Sahal-Bréchot, PhyS. 49 (1994) 34–38.

[18] C.G. Parigger, J.O. Hornkohl, L. Nemes, Appl. Opt. 46 (2007) 4026–4031.

[19] M. Cvejić, M.R. Gravilović, S. Jovićević, N. Konjević, Spectrochim. Acta Part B 85 (2013) 20–33.

[20] M. Cirisan, M. Cvejić, M.R. Gravilović, S. Jovićević, N. Konjević, J. Hermann, J. Quant. Spectrosc. Radiat. Transf. 133 (2014) 652–662.

[21] N. Omenetto, J.D. Winefordner, C.T.J. Alkemade, Spectrochim. Acta Part B 30 (1975) 335–341.

[22] W.L. Wiese, Line Broadening, in: R. H. Huddlestone, S. L. Leonard (Eds.), Plasma Diagnostic Techniques, Academic Press, New York, 1965, pp. 265–317.

[23] N. Konjević, Phys. Rep. 316 (1999) 339–401.

[24] H.Y. Moon, K.K. Herrera, N. Omenetto, B.W. Smith, J.D. Winefordner, Spectrochim. Acta Part B 64 (2009) 702–713.

[25] C. G. Parigger, A.C. Woods, M.J. Witte, L.D. Swafford, D.M. Surmick, J. Vis. Exp. 38 (2012) E51250.

[26] F. Bredice, F.O. Borges, H. Sobral, M. Villagran-Muniz, H.O. DiRocco, G. Cristoforetti, S. Legnaioli, V. Palleschi, L. Pardini, A. Salvetti, E. Tognoni, Spectrochim. Act. B 61 (2006) 1294–1303.

[27] M. Ivković, N. Konjeviæ, Z. Pavloviæ, J. Quant. Spectrosc. Radiat. Transf. 154 (2015) 1–8.

[28] G. Gautam, D.M. Surmick, C.G. Parigger, J. Quant. Spectrosc. Radiat. Transf. 160 (2015) 19–21.

[29] C.G. Parigger, Spectrochim. Acta Part B 79-80 (2013) 4–16.

[30] J. F. Kielkopf, N.F. Allard, J. Phys. B: At. Mol. Opt. Phys. 47 (2014) 155701.

[31] C.G. Parigger, D. M. Surmick, G. Gautam, A.M. EL Sherbini, Opt. Lett. 40 (2015) 3436–3439.

[32] J. J. Olivero, R. Longbothum, J. Quant. Spectros. Radiat. Transf. 17 (1977) 233–236.

[33] S.M. Abrarov, B.M. Quin, Appl. Math. Comp. 218 (2011) 1894–1902.

[34] M. Zaghloul, A. Ali, ACM Trans. Math. Soft. 38 (2011) 15:1–15:17.

[35] G.P.M. Poppe, C.M.J. Wijers, ACM Trans. Math. Soft. 16 (1990) 38–46.

[36] M. Abromowitz, I.A. Stegun, Handbook of Mathematical Functions with Formulas, Graphs, and Mathematical Tables, Dover, 1965.

[37] V. Fadeeva, N.M. Terentjev, Tables of values of the probability integral for complex arguments, State Publishing House for Technical and Technological Literature, Moscow, 1954.

[38] J. Nocedal, S. J. Wright, Numerical Optimization, Springer Verlag, Berlin, 2006.

[39] N.R. Conn, N.I.M. Gould, Ph.L. Tont, Tryst Region Methods, SIAM/MPS Series on Optimization, SIAM and MPS, Philadelphia, 2000.

[40] W.L. Wiese, N. Konjević, J. Quant. Spectros. Radiat. Transf. 28 (1982) 185–198.

[41] C.G. Parigger, G. Gautam, D.M. Surmick, Int. Rev. Atom. Mol. Phys. 6 (2015) 43–55.

[42] S. Eschlböck-Fuchs, A. Demidov, I.B. Gornushkin, T. Schmid, R. Rössler, N. Huber, U. Panne, J.D. Pedarnig, Spectrochim. Acta Part B 123 (2016) 59–67.

[43] N. Konjević, M. Ivkoviæ, S. Joviæeviæ, Spectrochim. Acta Part B 65 (2010) 593–602.

[44] D.M. Surmick, C.G. Parigger, Int. Rev. Atom. Mol. Phys. 5 (2014) 73–81.

[45] C.G. Parigger, L.D. Swafford, D.M. Surmick, M.J. Witte, A.C. Woods, G. Gautam, J. Phys. Conf. Ser. 548 (2014) 012043.

[46] D.M. Surmick, C.G. Parigger, J. Phys. B.: Atom. Mol. Opt. Phys. 48 (2015) 115701.

[47] J.P. Holtsmark, AdP 363 (1919) 577–630.

[48] A. Sapar, R. Poolamäe, L. Sapar, Baltic Astronomy 15 (2006) 435–447.

[49] C.G. Parigger, D.M. Surmick, G. Gautam, Self-absorption effects on line shapes in laser-induced plasma, in: Book of Abstracts, 23rd Int. Conf. Spectr. Line Shapes, Wydawnictwo Naukowe UMK, Toruñ, Poland, 2016, p. 102. http://icsls23.fizyka.umk.pl/, 2016 (accessed 15.09.2016).

[50] C.G. Parigger, D.M. Surmick, G. Gautam, Self-absorption characteristics of measured laser-induced plasma line shapes, J. Phys.: Conf. Ser. (2017) in press.

[51] F.E. Irons, J. Quant. Spectrosc. Radiat. Transf. 22 (1979) 1–44.